Inorganic Chemistry

Article

pubs.acs.org/IC

Chameleonic Nature of Hydroxyheme in Heme Oxygenase and Its Reactivity: A Density Functional Theory Study

Mahin Gheidi, Nasser Safari,* and Mansour Zahedi

Department of Chemistry, Faculty of Sciences, Shahid Beheshti University, G. C. Evin, 19839-63113 Tehran, Iran

Supporting Information

ABSTRACT: Iron hydroxyheme is an intermediate in heme degradation that binds to HO-1 in a five-coordinated fashion wherein the fifth ligand is His25. The structure and reactivity of hydroxyheme have been investigated using the B3LYP*, OPBE, and CASSCF methods with the 6-31+G* and 6-311+G** basis sets. Hydroxyheme $[(Im)Fe^{II}(POH)]$ (POH is the hydroxyporphyrin) is readily oxidized to oxophlorin $[(Im)Fe^{III}(PO)]$ (PO is the oxophlorin trianion) in the protein heme oxygenase. A computational study in the gas phase has shown that $^6[(Im)Fe^{II}(POH)]$ loses one electron from its a_{2u} orbital in the presence of O_2 and produces $[(Im)Fe^{II}(PO^{\bullet})]_{a_{2u}}$ ($PO^{\bullet}$ is the oxophlorin dianion radical) in the sextet ground state with a ferrous keto π-neutral radical structure and $d_{xy}^2a_{2u}^1d_{yz}^1d_{xz}^1\sigma^*_{z2}{}^1d_{x^2-y^2}^1$ electronic configuration. There is a closely lying exited state accompanying this ferrous keto π-neutral radical that has a high-spin ferric keto anion form of $^6[(Im)Fe^{III}(PO)]_{xy}$ with $a_{2u}^2d_{xy}^1d_{yz}^1d_{xz}^1\sigma^*_{z2}{}^1d_{x^2-y^2}^1$ electronic configuration. In the protein environment with a dipole moment larger than 5.7, the ground state is reversed and $^6[(Im)Fe^{III}(PO)]_{xy}$ is at least 1.47 kcal/mol lower than the ferrous π-neutral radical of $^6[(Im)Fe^{II}(PO^{\bullet})]_{a_{2u}}$. The interaction of H_2O, O_2, and CO with iron oxophlorin will shift the electronic structure toward the formation of a keto π-neutral radical resonance form in the following order: CO > O_2 > H_2O.

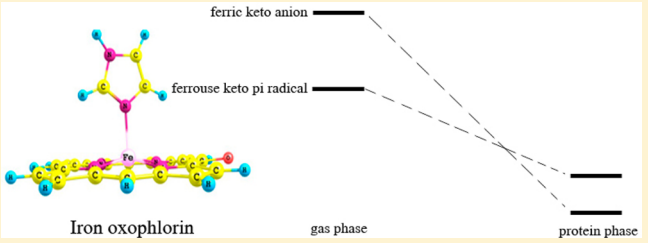

INTRODUCTION

Heme oxygenase (HO) is an important enzyme in human physiology involved in the degradation and recycling of heme iron.[1−7] Because less than 3% of our daily iron requirement comes from our diet, the rest must be made available through this recycling process.[8,9] In mammals, HO is a membrane-bound protein and is found in two forms: HO-1 and HO-2. The former mainly functions as the heme catabolism and antioxidant defense, while the latter is involved in the biosynthesis of carbon monoxide (CO), which functions as a neural messenger molecule in the brain.[10] HO catalyzes the conversion of ferric heme into iron biliverdin and CO in a multistep reaction mechanism, as displayed in Scheme 1. This stepwise mechanism uses three molecules of molecular oxygen and several electrons delivered by NADPH−cytochrome P450 reductase.[11] The conversion of ferric heme into *α-meso*-hydroxyheme (hydroxyheme) is believed to be carried out by an iron(III) hydroperoxo intermediate,[12−14] a reaction that is regioselective at the α position. This is imposed by the HO enzyme because of strict hindrance of the distal helix over the β, γ, and δ positions. The next step in the HO mechanism is the conversion of hydroxyheme into verdoheme in a multistep reaction that includes dioxygen (O_2) binding, O−O bond cleavage, CO liberation, and reorganization of the macrocycle, accompanied by several electron-transfer processes.[2,15,16] Because of the fact that this second multistep oxygenation is rapid and spontaneous in the presence of O_2, the details of ligation and the electronic and spin states of the reactive form of the iron hydroxyheme and its mechanism remain illusive.

Mansfield Matera et al.[15] have reported that this reaction simultaneously consumes one oxygen and an electron. Liu et al.[16] insisted that the oxygen molecule alone converts *α-meso*-hydroxyheme to ferric verdoheme and that the electron is used to reduce ferric verdoheme to the ferrous species. Sakamoto et al.[17] reported that the conversion of *α-meso*-hydroxyheme to ferrous verdoheme precedes the reduction of ferric *α*-hydroxyheme.

However, it is so far clear that iron(II) hydroxyheme is converted to iron(II) verdoheme and CO by one molecule of O_2. All α, β, γ, and δ isomers are rapidly converted to the corresponding isomers of verdoheme, and it seems that the HO enzymes have not been shown to play a critical role.[18] Therefore, hydroxyheme produces key intermediate substrates that are sometimes very reactive with O_2. In this step, surprisingly not only does CO not inhibit the conversion of hydroxyheme to verdoheme but it is also believed to lead to the production of an iron(II) keto π-neutral radical resonance structure, which enhances the hydroxyheme reactivity toward O_2.[15,16] In spite of these facts, the reactive intermediates in the conversion of hydroxyheme to verdoheme have not been thoroughly identified nor has the crystal structure of the *meso*-hydroxyheme−HO complex been resolved.

Received: February 8, 2013
Published: March 5, 2014

dx.doi.org/10.1021/ic402754y | Inorg. Chem. 2014, 53, 2766−2775

Scheme 1

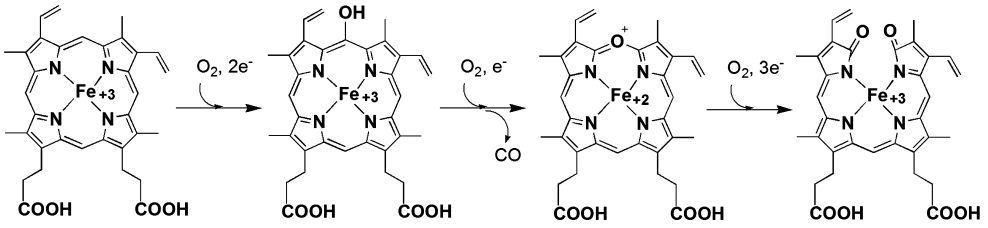

Scheme 2

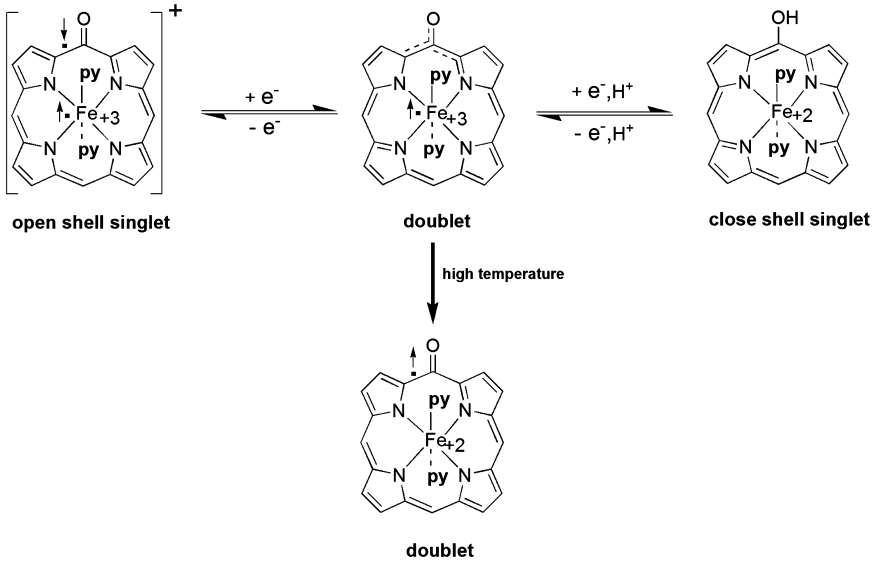

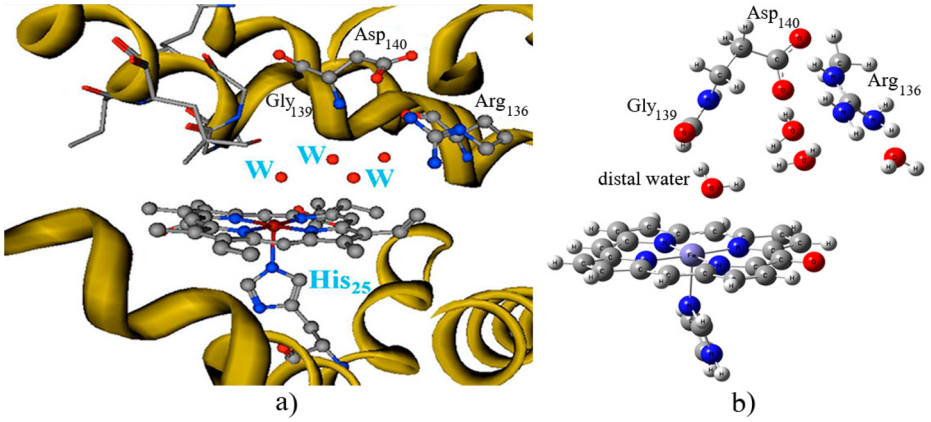

Figure 1. (a) Active-site structure of heme in HO as taken from the 1N3U PDB file. Amino acids are labeled as in the crystal structure, and W is a water molecule. (b) Corresponding structure used as the basis for our calculation.

Furthermore, Balch and co-workers have indeed shown that in the coupled oxidation process there is an ambiguity in view of the allotment of electrons distributed between the metal and ring of oxophlorin.[19−24] Experimental[25] and theoretical[26] investigations have also manifested that $^{2}[(Py)_2Fe^{III}(PO)]^0$ undergoes two reversible, one-electron processes. We have also illustrated that the electronic and spin distribution, oxidation state, and reactivity in six-coordinate iron oxophlorin were related to the axial ligands.[26,27] The oxidation of $^{2}[(Py)_2Fe^{III}(PO)]^0$ to $^{1,3}[(Py)_2Fe^{III}(PO^{\bullet})]^+$ occurred by removal of an electron from an a_{2u} orbital, in agreement with the experimental results (Scheme 2). Thus, the radical nature of the macrocycle in $[(Py)_2Fe^{III}(PO)]^0$, at higher temperatures, and in $[(Py)_2Fe^{III}(PO^{\bullet})]^+$, at lower temperatures, makes them very reactive toward O_2. Our question now is, what is the reactive form of hydroxyheme or oxophlorin in the natural HO system? To address this, we will discuss the details of our investigation into the electronic and spin states of the reactive form of five-coordinate biologically related hydroxyheme. These studies are the prerequisite for understanding the mechanism of its conversion.

dx.doi.org/10.1021/ic402754y | Inorg. Chem. 2014, 53, 2766−2775

Table 1. Calculated Relative Energies for Hydroxyhemes Using the B3LYP* and OPBE/6-311+G** Methods

	stabilization energy (kcal/mol)					
	B3LYP*			OPBE		
compound	low	intermediate	high	low	intermediate	high
^{1,3,5}(**1**)	9.81	1.35	0.00	7.50	0.68	0.00
^{6}(**2**)			3.42			
^{2,4,6}(**3**)	8.80	4.06	0.00	8.80	1.12	0.00
^{2,4,6}(**4**)	4.45	0.00	1.87	3.80	0.00	0.75
^{2,4,6}(**5**)	0.00	3.12	12.00	0.00	0.50	12.61
^{2,4,6}(**6**)	0.00	20.14	15.04	0.00	12.75	16.00

Model Used and Choice of Initial Geometries. Figure 1a displays the active site structure of heme in HO as taken from the 1N3U protein databank (PDB) file.[28] Ferrous heme is ligated to an axial histidine of His25 and is virtually planar. On the distal side of the heme, there is a water channel containing at least four crystal water molecules (W), which form a proton-relay chain connecting several proton donor groups, e.g., from Arg136, Asp140, and Gly139, to heme iron.[29] This water channel is located on the distal heme site above the α position of the heme ring. The amino acid helix blocks access to the β-, γ-, and δ-*meso* positions of the heme, which are shielded from this proton relay channel. Therefore, because of the lack of the hydroxyheme−HO structure, the α-C atom in heme has been replaced with the keto group in the heme−HO structure.

METHODS

All calculations were performed using previously described methods, which have been briefly summarized here.[26,27,30] The density functional theory (DFT) method was employed using the B3LYP* and OPBE hybrid density functional method, as implemented in the *Gaussian 2003* (A.B.3)[31] program series. The B3LYP* and OPBE[32,33]/6-31+G* methods were used for the optimization of all structures. The energies were corrected by single-point calculation with a larger basis set 6-311+G**[34,35] for all of the atoms and in all cases. Also, the complete active-space self-consistent-field (CASSCF)[36,37] wave functions with second-order multireference perturbation theory were analyzed to validate our DFT methods. The second-order perturbation theory (CAS MP2) energy corrections have been obtained for the CASSCF-level and DFT-optimized states, which use the CASSCF wave functions as the reference function. A modification of B3LYP to B3LYP*,[38,39] where the Hartree−Fock exchange was reduced by 5% (from 20% to 15%), was also used. The spin-unrestricted version of the B3LYP* (UB3LYP*) method was applied even to the singlet states when the reaction species were reasonably considered to have an open-shell singlet electronic configuration.[40−44] The iron(III) superoxo species (**5**, in the doublet state) has significant spin contamination, which leads to the possibility of contribution to an admixture of high-spin states. Spin contamination was studied, and the subtraction of the energy contribution of the higher spin states from the spin-contaminated energy was obtained.[45,46]

All energies reported in this work used the latter basis set and were corrected for zero-point energies, as taken from the frequency calculations. Atomic charge and spin-density studies were based on the Mulliken calculation. Natural bond orbital (NBO) analysis was used to explain the electron in the d orbitals of iron and the macrocycle ring as well as to assign the atomic charges. The molecular orbital analyses were performed by *GaussView* applied to the respective Gaussian output file. As an initial guess, an unrestricted Hartree−Fock calculation was performed. The natural orbitals from this unrestricted Hartree−Fock calculation are then used as starting orbitals for the CASSCF procedure. The CASSCF natural orbitals were visualized using the program *GaussView*.

The gas-phase energies were corrected using the self-consistent reaction field (SCRF) model[47] implemented with the 6-31+G* basis set at the gas-phase geometry. The two solvents were specified by a dielectric constant (ε), that is, ε = 5.7 with a dielectric medium for protein and ε = 24.55 under a stronger polarity for ethanol.

RESULT AND DISCUSSION

The experimental evidence shows that iron hydroxyheme bound to HO-1 is five-coordinate, wherein the fifth ligand is His25.[48−51] The difference between the chemical and enzymatic systems is the coordination state of iron hydroxyheme: six-coordinate in the model system and five-coordinate in the enzyme system. In this study, an ab initio DFT method was employed to investigate the electronic structure, spin states, and reactivity of the iron hydroxyheme complex in an environment similar to that of the HO system. The effects of H_2O, O_2, and CO on the reactivity of five-coordinate iron oxophlorin, which was formed from oxidation of hydroxyheme, in different oxidation and spin states were investigated in the heme degradation process (spin states are identified with a superscript before the label). Swart and co-workers[34,35] have shown that the B3LYP* and OPBE methods predict the high-spin ground-state energies in accordance with the experimental results and are superior to B3LYP. Furthermore, the OPBE method gives good results for iron complexes and other transition metals confirmed by Ghosh et al.[52−54] It is well-known that B3LYP overestimates the high-spin states and the 6-31+G* basis set predicts high-spin states that are low in energy. Therefore, the B3LYP* and OPBE methods with 6-31+G* and 6-311+G** basis functions have been employed in this investigation. Both methods were adequate for optimization of the structures and spin-state energies, yet in this work, it seems that B3LYP* can predict the electronic configuration especially for the high-spin ground state in these systems in accordance with the experimental evidence (see Table 1). We have also applied the CAS MP2/6-31G* calculation as a benchmark for the DFT results.

The geometries and energies of compounds ^{1,3,5}[(Im)-Fe^{II}(POH)] (**1**), ^{6}[(Im)Fe^{II}(PO$^{\bullet}$)] (**2**), ^{2,4,6}[(Im)Fe^{III}(PO)] (**3**), ^{2,4,6}[(Im)(H_2O)Fe^{III}(PO)] (**4**), ^{2,4}[(Im)(O_2^-)Fe^{III}(PO$^{\bullet}$)] (**5**), and ^{2,4,6}[(Im)(CO)Fe^{II}(PO$^{\bullet}$)] (**6**) were fully optimized and computed in all possible spin states. Table 1 shows the computed relative stabilization energies for these compounds. The compound numbering system in Scheme 3 has been preserved in this study. The charge densities and spin distributions for all compounds are presented in Table 2. The details of the bond distances for all compounds by the B3LYP* and OPBE methods are presented in the Supporting Information (SI). The results of this study were reexamined and validated by the CASSCF method. The obtained results from the CASSCF-level and MP2-corrected energies for all of

dx.doi.org/10.1021/ic402754y | Inorg. Chem. 2014, 53, 2766−2775

Scheme 3

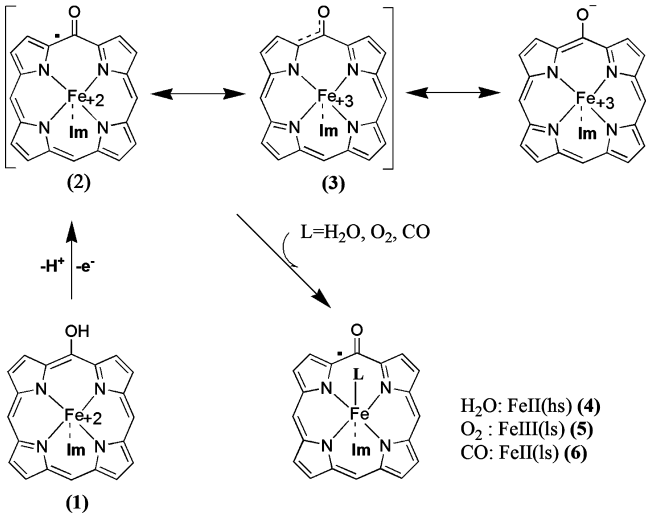

the species are listed in Tables S2 and S3 in the SI and confirm the DFT results.

Different resonance structures were proposed for the reactive form of hydroxyheme or oxophlorin. The experimental evidence indicates[16] that small molecules such as CO, O_2, and H_2O could dramatically change the stable resonance structures, oxidation, electronic configurations, and spin states of Fe and the macrocycle (Scheme 3).

Five-Coordinate Iron Hydroxyheme: Model for the Enzyme System. Experimental data indicate[15,48−51] that the heme−HO complex is five-coordinate possibly with an OH^- or H_2O in the distal position of the heme. The details of the electronic and spin states of this five-coordinate species have not been thoroughly identified.

Therefore, the model used in the five-coordinate iron hydroxyheme complex was based on the crystal structure shown in Figure 1, whereby all side chains of the macrocycle were replaced by H atoms and the α-C atom in the heme was replaced by a keto group. The proximal histidine in the HO complex is a neutral imidazole due to the one similarity seen with myoglobin rather than the imidazolate seen in peroxidase enzymes.[55]

Oxidation Reactions of Ferrous Hydroxyheme Complex 1. The geometry and energy of the five-coordinate ferrous hydroxyheme complex **1** were fully optimized and computed in singlet, triplet, and quintet states. The quintet spin state (ground state with $d_{xy}^2a_{2u}^2d_{yz}^1d_{xz}^1\sigma^{*1}_{z^2}\sigma^{*1}_{x^2-y^2}$ occupation) is 1.35 and 9.81 kcal/mol more stable than the triplet and singlet spin states, respectively, at the B3LYP*/6-311+G** level (Table 1 also shows the data for the OPBE method that is in accordance with the B3LYP* method). Subsequently, the oxophlorin complex of [(Im)Fe(PO)] is easily formed by losing one electron and a proton from **1**.

The oxidized species [(Im)Fe(PO)] was also fully optimized in all possible spin states using the B3LYP* and OPBE/6-31+G* methods. In this complex, the sextet spin state (ground state) is 4.06 kcal/mol more stable than the quartet spin state and 8.80 kcal/mol more stable than the doublet spin state at the B3LYP*/6-311+G** level (Table 1 also shows the data for the OPBE method that is in accordance with the B3LYP* method). In the sextet state, two possible electronic configurations are $d_{xy}^2a_{2u}^1d_{yz}^1d_{xz}^1\sigma^{*1}_{z^2}\sigma^{*1}_{x^2-y^2}$ and $a_{2u}^2d_{xy}^1d_{yz}^1d_{xz}^1\sigma^{*1}_{z^2}\sigma^{*1}_{x^2-y^2}$; these have been labeled as $^6[(Im)\text{-}Fe^{II}(PO^{\bullet})]_{a_{2u}}(^6\Psi_{a2u})^6$(**2**) and $^6[(Im)Fe^{III}(PO)]_{xy}(^6\Psi_{xy})^6$(**3**), respectively. The complex **3** state lies at only 3.42 kcal/mol higher than the radical species **2**. Form **2** includes an electron transfer from the doubly occupied d_{xy} orbital to a singly occupied a_{2u} orbital ($d_{xy} \rightarrow a_{2u}$), which leads to complex **3**. The electron distribution in the a_{2u} orbital of the oxophlorin has a π^* character located on the C−O bond, as has been indicated in Figure 2a. Because of this charge transfer from iron(II) to the oxophlorin ring, the C−O bond distance of **3** is elongated by about 0.04 Å (see Figure 2b).

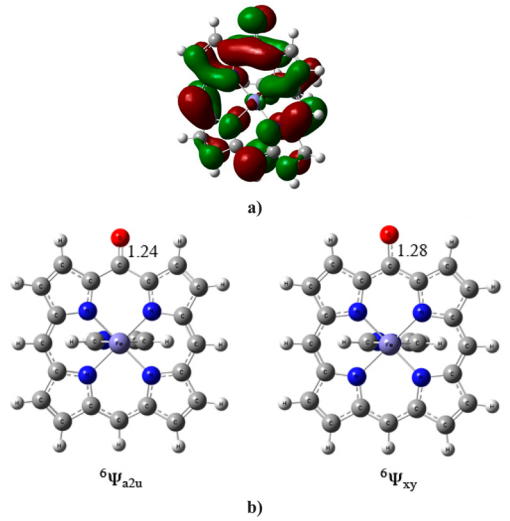

Figure 2. Oxophlorin complex of [(Im)Fe(PO)]: (a) Kohn−Sham HOMO with a_{2u} symmetry; (b) two optimized structures with different electronic aspects.

Therefore, our calculations show that the deprotonated species of [(Im)Fe(PO)] can be represented in the ground state as ferrous keto π-neutral radical resonance form ^{6}(**2**), which has a closely-lying excited state of ferric keto anion form ^{6}(**3**) in the gas phase.

Table 2. Calculated Mulliken Charges and Spin Densities for the Fe, O, C_{oxo}, and C_{meso} Atoms and the Ring Macrocycle (Values in Parentheses Are Charge Densities)

compound	Fe	ring	O	C_{oxo}	*meso*-C	*meso*-C trans
^{5}(**1**)	3.86 (1.17)	0.13 (−1.15)	0.00 (−0.23)	0.02 (0.20)	0.00 (0.00)	0.01 (0.03)
^{6}(**2**)	4.12 (1.19)	0.85 (−1.17)	0.25 (−050)	0.15 (0.23)	0.10 (0.00)	0.27 (0.05)
^{6}(**3**)	4.75 (1.46)	0.22 (−1.48)	0.02 (−0.64)	0.03 (0.26)	0.00 (0.06)	0.01 (0.06)
^{6}(**4**)	3.92 (1.20)	0.87 (−1.19)	0.26 (−0.46)	0.15 (0.26)	−0.09 (0.00)	0.28 (0.03)
^{2}(**5**)	1.08 (1.47)	0.92 (−1.24)	0.29 (−0.53)	0.15 (0.24)	0.10 (0.05)	0.28 (0.06)
^{2}(**6**)	0.00 (1.12)	1.00 (−0.95)	0.30 (−049)	0.15 (0.23)	0.12 (0.00)	0.28 (0.05)

dx.doi.org/10.1021/ic402754y | Inorg. Chem. 2014, 53, 2766−2775

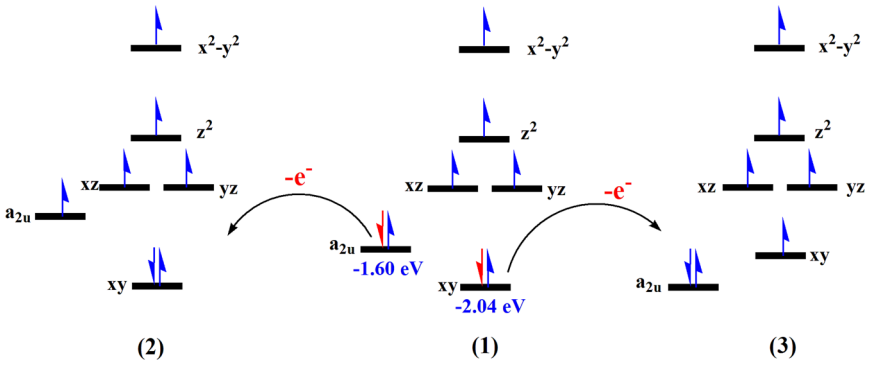

Figure 3. Energy-level diagrams for oxidation of the ferrous hydroxyheme complex **1**.

Our calculations in the gas phase show that the ferrous complex **2** is easily formed by one electron and a proton lost from the ferrous hydroxy form **1** at low positive potentials (with ionization energies = 8.66 kcal/mol). The oxidation takes place by the loss of one electron from the a_{2u} highest occupied molecular orbital (HOMO) of complex **1** (a_{2u}, −1.60 eV), and because of electron transfer that occurs mainly on the ring, the iron positive charge remains fixed at around 1.19, which is consistent with formation of the iron(II) oxidation state (see Table 2). However, one-electron oxidation of ferrous hydroxy complex **1** to ferric complex **3** occurs at higher positive potentials with ionization energies = 12.08 kcal/mol in the gas phase. In this case, an electron is removed from the d_{xy} HOMO of ferrous hydroxy complex **1** (d_{xy}, −2.04 eV) and has caused the charge density on the iron to increase from around 1.17 in ferrous hydroxy **1** to 1.46 in ferric complex **3** (see Figure 3).

Similar to our previous finding for model six-coordinate oxophlorin[27] and also the proposed oxidation of hydroxyheme to oxophlorin by Ortiz de Montellano et al.[16] and Morishima et al.,[56] we have found that the ferrous hydroxy form **1** in Figure 3 can also be easily oxidized to form a reactive iron oxophlorin by O_2.

The charge densities and spin distributions for the species **2** and **3** are reported in Table 2. In form **2**, the ring has a radical nature because the charge density and spin distribution on the oxophlorin ring are −1.17 and 0.85 and on the O atom are −0.50 and 0.25, respectively. In form **3**, the charge on the oxophlorin is −1.48 (O = −0.64) and the spin density is 0.22 (O = 0.02). Therefore, the electron density is transferred from the oxophlorin ring to the iron center, which leads to the iron(II) π dianion radical species **2**. The radical nature of the macrocycles in species **2** possibly makes the iron oxophlorin complex a reactive species in the heme catabolism. In the ferrous complex (**2**), four unpaired electrons are localized on the ferrous ion, and the fifth unpaired electron is on the macrocycle with the same spin (the spin density on the iron is 4.12, and that on the macrocycle is 0.85; see Table 2). To confirm the electronic configurations, NBO analysis for **2** is presented in Table 3a. This evidence also demonstrates that in iron the occupancy number of α spin orbitals is 4.73 and that of the β spin orbitals is 0.87, which results in a net α spin of 3.86 on the iron. Almost one unpaired electron with α orientation is localized on the ring to make a sextet [Fe^{II}($PO^{\bullet}$)] d^6 system.

Effect of the Solvent and Medium. The significance of solvation on polar and charged species is well recognized. The details for solvation data are presented in the SI.

In Figure 4, we show the significant difference between the gas-phase and protein behavior. In the gas phase, all of the oxidation processes are more endothermic. This trend makes sense because charge species are stabilized by solvation. Therefore, Figure 4 shows that, in a polar medium, all of the oxidation processes have lower oxidation potentials than those of the gas phase. The oxidation potentials of complex **1** to species **3** and **2** in a medium with ε = 5.7, which is proposed for protein environments, reduce to 3.35 and 4.82 kcal/mol, respectively. In a medium of higher polarity such as ethanol with ε = 24.55, further reduction to 1.78 and 4.36 kcal/mol occurs for species **3** and **2**, respectively. Solvation puts a stronger impact on the ferric complex **3** and changes the gas-phase ground state of the ferrous complex **2** to the high-spin ferric complex **3**. On the basis of the charge density calculations (see Table 2) in form **3**, the charge densities on iron and oxygen are 1.46 and −0.64, respectively, while in form **2**, the charge densities are 1.19 and −0.50. Therefore, in the protein and polar environments, the formation of the ferric species **3** is considerably more facile than that of the gas phase. Therefore, in the protein environment with a dipole moment larger than 5.7, the ground state is the high-spin ferric complex **3**, which is at least 1.47 kcal/mol lower than the ferrous π-neutral radical **2**.

In conclusion, an external electric field is able to change the electronic system from an oxophlorin-based radical **2** to an oxophlorin-based trianion **3**. This shows that iron oxophlorin systems are chameleonic species that are influenced by external perturbations and change their character and reactivity depending on the local environment. Interestingly, these observations are quite confirmatory and also complementary

Table 3. NBO Analysis of the Electron Distribution in the Iron Atom of (a) ^{6}2 and (b) ^{2}6

α spin orbital		β spin orbital	
occupancy	orbital	occupancy	orbital
(a) ^{6}2			
0.99018	LP (1)Fe	−0.87101	LP (1)Fe
0.98415	LP (2)Fe		
0.95966	LP (3)Fe		
0.90119	LP (4)Fe		
0.89500	LP (5)Fe		
sum of the α spin electron		sum of the β spin electron	
4.72881		−0.87101	
(b) ^{2}6			
0.97423	LP (1)Fe	−0.92304	LP (1)Fe
0.97117	LP (2)Fe	−0.91250	LP (2)Fe
0.95360	LP (3)Fe	−0.84402	LP (3)Fe
sum of the α spin electron		sum of the β spin electron	
2.89900		−2.67956	

dx.doi.org/10.1021/ic402754y | Inorg. Chem. 2014, 53, 2766−2775

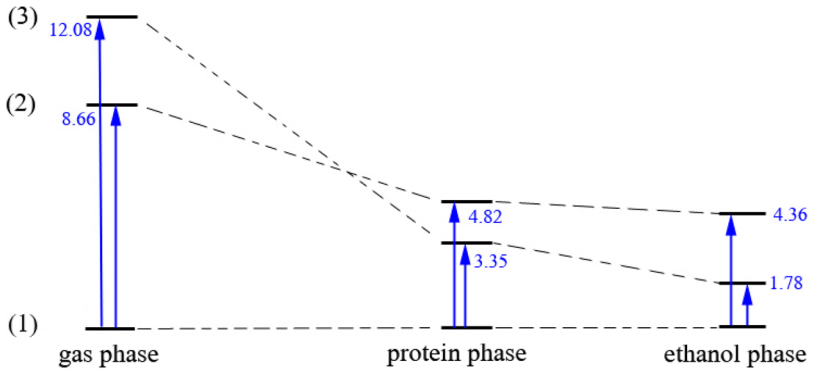

Figure 4. Schematic representation of the solvent effect with medium and strong polarity on the oxidation potentials of iron hydroxyheme in kcal/mol.

to the experimental results. Ortiz de Montellano, Mansfield Matera, and Masato Noguchi[15−17] have shown that ferric oxophlorin formed in HO shows a high-spin iron(III) signal accompanied with an organic radical. Electron paramagnetic resonance (EPR) and Raman studies both confirm the existence of species **3** and **2**, in which the latter compound will dominate under exposure to CO.

Effect of the Distal Water on the Orbital Energy Levels, Spin States, and Reactivities of Iron Oxophlorin. In the crystal structure of heme, the distal ligand is usually a water molecule.[57] The water molecule is anchored by a hydrogen-bonding interaction with Asp140 and also forms a hydrogen-bonding network involving Gly139 and Arg136 (Figure 1).

As shown in Figure 1b, the active site of the intermediate of hydroxyheme was chosen as an iron hydroxyheme complex (without side chains of heme and by replacement of an α-C atom in heme with a keto group) with its proximal ligand His25 (modeled as imidazole) and a few key protein residues: Arg136 [modeled as $CH_3NHC^+(NH_2)_2$], Asp140 [modeled as $NHCH_2CH_2COO^-$], and Gly139 (HCO). Four crystal waters were included that form a water cluster through a hydrogen-bonding network in the distal pocket taken from the 1N3U PDB file.[28] The distance of the distal water to the iron center is about 2.70 Å. To test the effect of the environment, we performed single-point calculations using the 6-31+G* basis set on iron and 6-311+G** on the rest of the atoms. The relative stabilization energy of the active-site iron hydroxyheme in HO was computed in doublet, quartet, and sextet states, and the sextet spin state (ground state) is 5.03 and 9.48 kcal/mol more stable than the quartet and doublet spin states, respectively.

Subsequently, in this work, the H_2O is approached the iron from the opposite site of imidazole in different orientations as the sixth axial ligand. The structure of $[(Im)(H_2O)Fe^{III}(PO)]$ (**4**) was optimized by DFT methods. The presence of the H_2O as the sixth axial ligand caused elongation of the Fe−N bond distance to 2.22 Å, which is unexpectedly larger than that of the Fe−N distance (2.16 Å) in the five-coordinate complex of $[(Im)Fe^{III}(PO)]$. This shows that σ bonding is delocalized over the entire N_{im}−Fe−O moiety. Elongation of the Fe−O linkage will be accompanied by N_{im}−Fe shortening, a trans effect. Thus, the protein and its interaction with the Fe−H_2O moiety of the active species cause a shift in the spin density of iron oxophlorin. The effect of the distal water on iron oxophlorin changes the high-lying occupied and low-lying virtual orbital energy levels.

Figure 5 shows the relaxed scan along the Fe−H_2O coordinate for elongation of the Fe−O distance in complex **4**

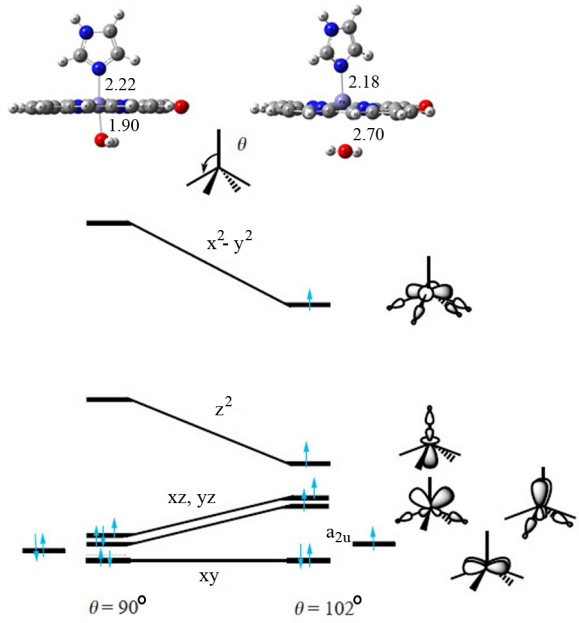

Figure 5. Correlation diagram for the d-block orbitals of complex **4**, with the angle θ varying from 90° to about 102° in the course of the scan of the Fe−H_2O bond.

in all possible spin states. With elongation of the Fe−O distance, in the sextet energy surface, stabilization of the ferrous π radical resonance, $^6[(Im)(H_2O)Fe^{II}(PO^{\bullet})]$ [^{6}(**4**)], is increased because the energy surfaces of the singly occupied d_{z^2} and $d_{x^2-y^2}$ orbitals are decreased, while in the doublet energy surface, stabilization of $^2[(Im)(H_2O)Fe^{III}(PO)]$ [^{2}(**4**)] with elongation of the Fe−O distance is decreased because the energy surfaces of d_{xz} and d_{yz} HOMOs are increased. In Figure 5, we present a schematic correlation diagram that shows the changes to the shape and energy of the d-block orbitals during this geometrical deformation as the angle θ varies from 90° to about 102°. The *xz* and *yz* orbitals, which are nonbonding in θ = 90° with Fe−O = 1.90 Å (in the low-spin state), are therefore destabilized in θ > 90° with Fe−O > 2.00 Å (in the high-spin state), with their energy rising as the overlap with the ligand orbital increases. It must be noted that a crossing between the energy levels of the orbitals that are destabilized (*xz* and *yz*)

dx.doi.org/10.1021/ic402754y | Inorg. Chem. 2014, 53, 2766−2775

and the z^2 orbital, which is stabilized, can occur if θ and the Fe−O bond distance become sufficiently large.

The radical nature of the macrocycles in complex ^{6}(**4**) (hydroxyheme with the distal water at a distance of 2.70 Å from the iron atom) possibly makes it more reactive toward O_2 by the spin-allowed path (see Figure 5), an effect that may have been inserted by the flexibility of the protein HO moiety.

*Iron(III) Superoxo Oxophlorin (**5**).* In the five-coordinate ferrous complex **2**, the z^2 orbital is polarized and stabilized in comparison with the six-coordinate complex (see Figure 6).

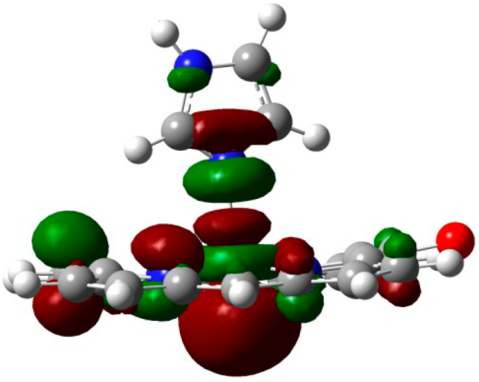

Figure 6. Kohn−Sham orbital for the d_{z^2} SOMO of the five-coordinate complex ^{2,4,6}(**2**), which shows the polarized d_{z^2} orbital.

Then the z^2 orbital of **2** is singly occupied in all spin states and is reactive toward $^3O_2$ according to the spin rule. Thus, coordination of O_2 as a sixth ligand to the iron is a possibility.

The oxyiron species is remarkable because the two constituents **2** and $^3O_2$ have a total of seven unpaired spins to begin with, and all of these spins couple in the iron(III) superoxo species **5**, which is known to be a doublet or quartet state species. Results show that for these species the doublet state (ground state) is 3.12 kcal/mol more stable than the quartet state.

The HOMOs are shown in Figure 7 and originate from the iron and O_2 orbitals. The lowest lying d-type orbital is the δ_{xy} orbital, which is nonbonding and located in the plane of the hydroxyheme. Higher in energy are two orthogonal pairs of π^*_{xz} and π^*_{yz} orbitals for the antibonding interaction of $3d_{xz}$/$3d_{yz}$ on iron with $2p_x$/$2p_y$ on oxygen. In addition, there are two virtual σ^*-type orbitals for the antibonding interactions of the metal with hydroxyheme ($\sigma^*_{x^2-y^2}$) and with the axial and distal ligands ($\sigma^*_{z^2}$). Finally, there is a π^*_{OO} orbital for the antibonding interaction along the O−O bond.

In species **5**, this set of orbitals is occupied with seven electrons. The electronic ground state is a doublet state with orbital occupation $\delta_{xy}{}^2\pi^*_{xz}{}^2\pi^*_{yz}{}^1\pi^*_{OO}{}^1\pi_{a_{2u}}{}^1$, whereby the unpaired electrons are antiferromagnetically coupled; hence, there are five metal-based electrons connected to a superoxo group. Therefore, we characterize species **5** as an iron(III) superoxo complex. This orbital occupation resembles that of the iron(III) superoxo intermediate in the catalytic cycle of cytochrome P450.[58−60]

Species ^{4}(**5**) has the same orbital occupation as the doublet spin ground state and therefore also corresponds to an iron(III) superoxo complex with three unpaired electrons. Optimized geometries of the iron(III) superoxo complex in the doublet and quartet states are nearly degenerate. Table 2 shows species ^{2,4}(**5**) with one unpaired electron in the iron and a second

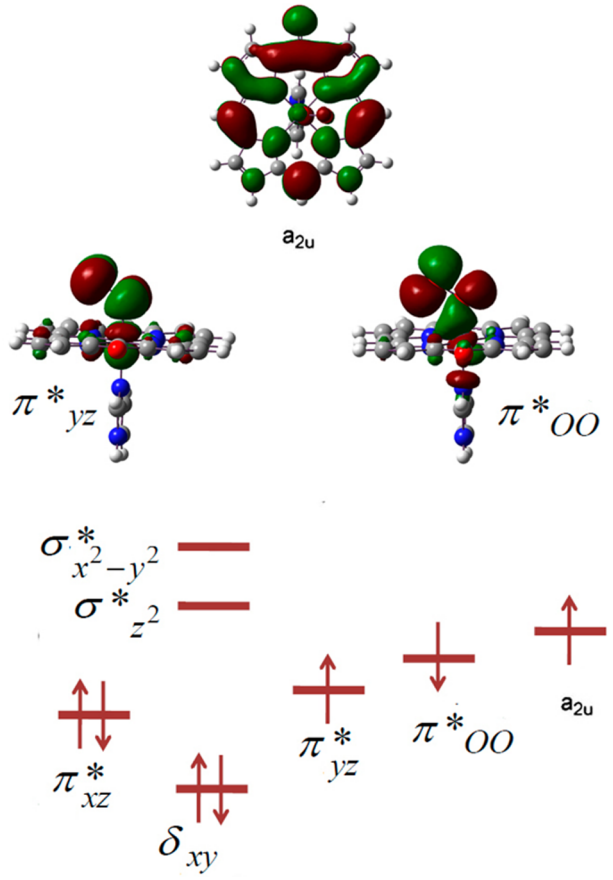

Figure 7. Kohn−Sham orbitals for the last five HOMOs of complex ^{2}**5**.

unpaired electron on the macrocycle ligand, with the same spin to the iron ready for bond formation with spin pairing of oxygen and macrocycle (the spin density on the iron is 1.08 and that on the macrocycle is 0.92). The terminal oxygen atom has one unpaired electron (spin density −0.71), with opposite spin coupled to the other unpaired electron, leading to a system with three radicals and a doublet spin state (see Figure 7). The spin-density plot indicates that ^{2,4}**5** may be explained as an antiferro- and ferromagnetically coupled Fe $^{III}(S = {}^1/_2)O_2{}^{\bullet}PO^{\bullet 2-}$ electronic configuration (Figure S1 in the SI).[61] The radical nature of iron oxophlorin in this complex makes it vulnerable to nucleophilic attack by the terminal oxygen atom. Spin contamination was examined and a $\langle S^2\rangle$ value of 1.85 was achieved for ^{2}(**5**), which is considerable and confirmatory of single occupation of the π^*_{yz} and π^*_{OO} orbitals that are considered as two orbitals of the Fe−O_2 moiety (see Figure 7) or a contribution to an admixture of high-spin states. After spin correction, complex ^{2}(**5**) has been destabilized about 1.5 kcal/mol, resulting in lower doublet−quartet splitting, and that is another indication of the admixture of doublet−quartet states in this species. On basis of calculations of the spin density and molecular orbital, **5** could possibly have an EPR-silent iron (with two unpaired electrons) and a radical signal relevant to the π-neutral radical macrocycle.[15,16]

*[(Im)(CO)Fe^{II}(PO$^{\bullet}$)] (**6**).* Full optimization of the electronic structure of **6** was performed, and the parameters have been collected in the SI. Optimized geometries ^{4}(**6**) and ^{6}(**6**) are 20.14 and 15.04 kcal/mol higher in energy than the doublet spin ground state, respectively. In the doublet spin state

dx.doi.org/10.1021/ic402754y | Inorg. Chem. 2014, 53, 2766−2775

(ground state), the Fe−C distance is 1.77 Å and the average Fe−N_{eq} distance is 2.03 Å, which stabilized the low-spin iron(II) state. CO coordination caused the ferrous π radical form ^{2}(**6**) to absolutely dominate, as is well documented by EPR evidence from experimental work.[16] Figure 8 shows the

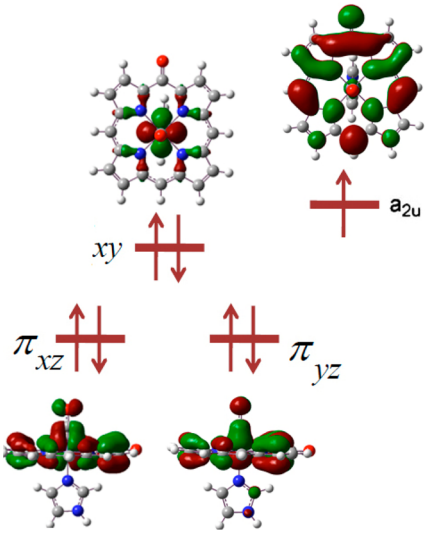

Figure 8. Kohn−Sham orbitals for the last four HOMOs of ^{2}**6**.

Kohn−Sham orbitals for the last four HOMOs of ^{2}(**6**). On the basis of this figure, an unpaired electron is placed on the a_{2u}-like orbital of the macrocycle and the electronic configuration of iron is $d_{xy}^2(\pi_{xz},\pi_{yz})^4$. Therefore, the ring of the aforementioned complex has a radical nature because the charge density on the oxophlorin is −0.95 and the spin distribution is 1.00. However, as shown in Figure 8, one of the electrons is shifted from the macrocycle ring to iron in ^{2}(**6**), which results in the iron(II) π dianion radical species. Upon exposure to O_2, this radical reacts with O_2 to yield iron(III) verdoheme with no requirement for exogenous reducing equivalents.[17] This is a rare example of CO activation of iron to react with O_2. CO released during the conversion of oxophlorin to verdoheme results in the higher reactivity of oxophlorin.

Calculated spins show that the spin density on the iron is 0.00 and that on the tetrapyrrole ligand is 1.00 (see Table 2 and Figure S2 in the SI). This electronic distribution is in accordance with the metal orbital splitting shown in Figure 8. Data from analysis of NBO in Table 3b also show that the occupancy number of the α spin orbital for iron is 2.91 and that of the β spin orbital for iron is 2.68, which results in a net α spin of 0.23 on iron. Almost one unpaired electron with α is present on the macrocycle to make the whole system an iron(II) d^6 with the macrocycle as a dianionic radical.

CASSCF Study. To further confirm the electronic structures of the oxidized species [(Im)Fe(PO)] and iron(III) superoxo species **5**, we performed CASSCF with second-order perturbation theory calculation. We chose a minimal active space that contains all orbitals that are possibly relevant for a correct description of the spin density and electronic configuration. The total energies and Mulliken spin densities are listed in Tables S2 and S3 in the SI. The natural orbitals obtained in these minimal CAS(7e,7o) calculations are also shown in Figure 9. These results are in an active space composed of five iron 3d orbitals and the a_{2u} orbital of the oxophlorin. In addition, the a_{1u} orbital has to be included in

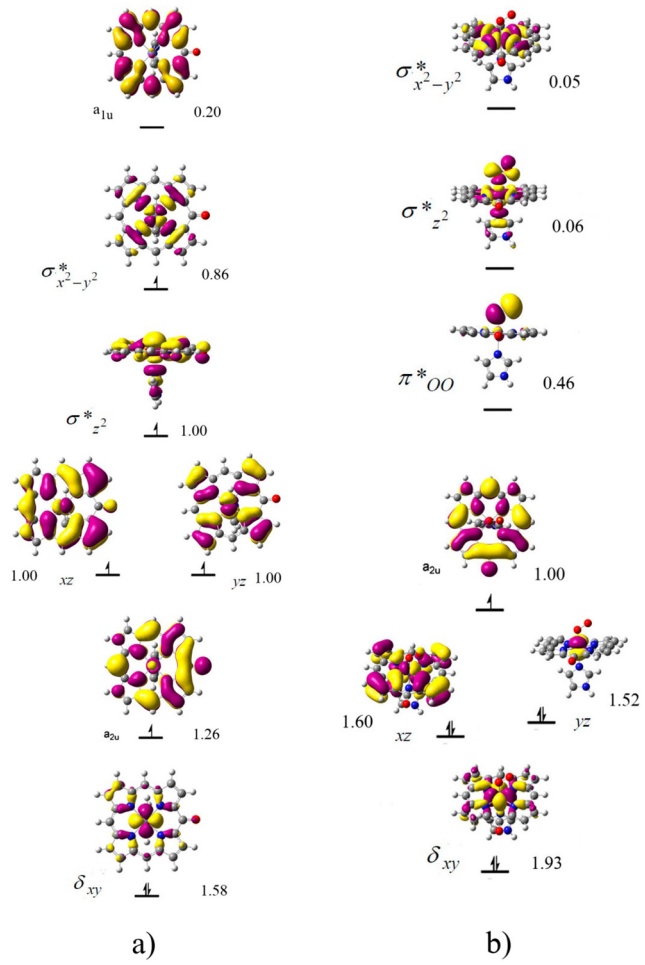

Figure 9. Natural orbitals and occupation numbers (a) for CAS(7e,7o) calculations of the sextet-state configuration of [(Im)Fe(PO)] and (b) for CAS(7e,7o) calculations of the doublet-state configuration of [(Im)Fe(PO)O_2].

[(Im)Fe(PO)] and the O_2 π^* orbital has to be included in iron(III) superoxo species **5**.

The total energies of [(Im)Fe(PO)] were computed in doublet, quartet, and sextet states (given in Table S2 in the SI) and show that the sextet state is the ground state. Table 4 lists the most important configurations for the sextet state. There is a dominant contribution to the wave function [configuration interaction (CI) weight > 0.7], which corresponds to the sextet ground state; all other CI coefficients are smaller but significant

Table 4. Total Wave Functions for the Sextet State of [(Im)Fe(PO)] and the Doublet State of [(Im)Fe(PO)O_2] in CAS(7e,7o)

[(Im)Fe(PO)] (S = $^5/_2$)		[(Im)Fe(PO)O_2] (S = $^1/_2$)	
1aaaaa0	0.75242891	**111a000**	0.64904386
a1aaaa0	−0.28072147	**11aab00**	−0.30576160
1aaaa0a	−0.24774226	**1a1ab00**	0.27597028
a1aaa0a	0.21206988	**1b1aa00**	0.23339070
a1aa0aa	0.09242891	**11baa00**	−0.10948772

[a]On the left-hand side, the configurations are printed; on the right-hand side, the corresponding CI coefficients are given. 1 = doubly occupied orbital. a = orbital occupied by an α electron. b = orbital occupied by a β electron. 0 = empty orbital.

dx.doi.org/10.1021/ic402754y | Inorg. Chem. 2014, 53, 2766−2775

(<0.3). This principal configuration is also shown in Figure 9a. The principal configuration contains four unpaired electrons on the iron atom and one unpaired electron on the macrocycle (π-neutral radical), which is in accordance with a $d_{xy}^2 a_{2u}^1 d_{yz}^1 d_{xz}^1 \sigma^*_{z^2}{}^1 \sigma^*_{x^2-y^2}{}^1$ electronic configuration ($^6\Psi_{a_{2u}}$). The polarization can be accounted for by adding those configurations that contain excitations from a d_{xy} HOMO to a_{2u} singly occupied molecular orbital (SOMO), meaning that the β electron density shifts toward the macrocycle ring. All of these excitations correspond to medium-sized CI coefficients (>0.09). Hence, these excited configurations lead to an excess of the α electron density on the iron atom, which leads to $^6\Psi_{xy}$ with orbital occupation $a_{2u}^2 d_{xy}^1 d_{yz}^1 d_{xz}^1 \sigma^*_{z^2}{}^1 \sigma^*_{x^2-y^2}{}^1$. Furthermore, for most excited configurations with large CI coefficients, the d_{xy} orbital remains singly occupied. These excited configurations are shown in Table 4.

The total energies of [(Im)Fe(PO)O_2] were also computed in doublet and quartet states. The doublet state with the $d_{xy}^2 d_{xz}^2 d_{yz}^2 a_{2u}^1$ electronic configuration is the ground state. Table 4 shows the most important configurations for the doublet state. There is a dominant contribution to the wave function (CI weight > 0.6), which is included in Figure 9b. The principal configuration however, which contains one unpaired electron on the macrocycle, cannot explain the observed spin polarization (Figures 7 and S1a in the SI). In addition, we find configurations that correspond to excitations from the d_{yz} or d_{xz} HOMO to the antibonding OO π^* virtual orbital, which shifts the β electron density toward O_2. Hence, these excited configurations lead to an excess of the α electron density on the iron atom and an excess of the β electron density on the OO fragment. It should be noted that, in all of the excited configurations listed in Table 4, the a_{2u} orbital is each singly occupied by one α electron and the π^*_{OO} orbital is each singly occupied by one β electron.

The occupation numbers in Figure 9 prove the electronic configuration of the species mentioned above, which is in agreement with our results obtained from DFT calculations. For example, in species ^{2}(**5**), the occupation number of d_{yz} is 1.52 instead of the expected 2. In addition, the occupation number of the π^*_{OO} virtual orbital is 0.46. This shows that one electron can arise from the iron atom to the π^*_{OO} orbital, which lead to species ^{2}(**5**) with orbital occupation $\delta_{xy}^2 \pi^*_{xz}{}^2 \pi^*_{yz}{}^1 \pi_{a2u}{}^1 \pi^*_{OO}{}^1$ (the unpaired electrons are antiferromagnetically coupled).

CONCLUSION

In conclusion, we found that the deprotonated ferrous species **2** is essential for the subsequent reaction with O_2 to yield verdoheme and to cleave the porphyrin ring because this radical species is highly reactive toward O_2. In the solution phase, the heme catabolism process is facilitated because of the lower oxidation potential. An external electric field is able to change the electronic system from an oxophlorin-based radical to an oxophlorin-based trianion. This shows that the reactivity of iron oxophlorin systems is influenced by external perturbations. O_2 and CO reactivates the oxophlorin ring while shifting the resonance structures toward a keto π-neutral radical form. To briefly summarize, oxygen and released CO during the catabolism process will activate more hydroxyheme substrates for further conversion to verdoheme. Furthermore, flexibility in the heme pocket, especially the distal water, helps the reactivity of hydroxyheme in the active site. Details of the nature of the macrocycle now open the route for investigation of the mechanism of this conversion that is under consideration in our laboratory.

ASSOCIATED CONTENT

Supporting Information

Cartesian coordinates, calculated selected bond distances, additional structures, calculated energies and Mulliken spin densities, and oxidation potentials. This material is available free of charge via the Internet at http://pubs.acs.org.

AUTHOR INFORMATION

Corresponding Author

*E-mail: n-safari@sbu.ac.ir. Tel.: +98-21-22401765. Fax: +98-21-22403041.

Notes

The authors declare no competing financial interest.

ACKNOWLEDGMENTS

We are grateful to Prof. S. W. Ng for providing us with the *Gaussian* software suite of programs and hardware (machine time) facilities and for providing us the opportunity to access some new features of the Gaussian products. The authors also acknowledge financial support from the Research Council of Shahid Beheshti University. Technical support of the Chemistry Computational Center at Shahid Beheshti University is also gratefully acknowledged.

REFERENCES

(1) Sono, M.; Roach, M. P.; Coulter, E. D.; Dawson, J. H. *Chem. Rev.* **1996**, *96*, 2841−2888.
(2) Ortiz de Montellano, P. R. *Acc. Chem. Res.* **1998**, *31*, 543−549.
(3) Poulos, T. L.; Li, H.; Raman, C. S.; Schuller, D. J. *Adv. Inorg. Chem.* **2000**, *51*, 243−294.
(4) Ortiz de Montellano, P. R.; Wilks, A. *Adv. Inorg. Chem.* **2000**, *51*, 359−407.
(5) Colas, C.; Ortiz de Montellano, P. R. *Chem. Rev.* **2003**, *103*, 2305−2332.
(6) Unno, M.; Matsui, T.; Ikeda-Saito, M. *Nat. Prod. Rep.* **2007**, *24*, 553−570.
(7) Matsui, T.; Unno, M.; Ikeda-Saito, M. *Acc. Chem. Res.* **2010**, *43*, 240−247.
(8) Uzel, C.; Conrad, M. E. *Semin. Hematol.* **1998**, *35*, 27−34.
(9) Foresti, R.; Motterlini, R. *Free Radical Res.* **1999**, *31*, 459−475.
(10) Maines, M. D. *Annu. Rev. Pharmacol. Toxicol.* **1997**, *37*, 517−554.
(11) Schacter, B. A.; Nelson, E. B.; Marver, H. S.; Masters, B. S. *J. Biol. Chem.* **1972**, *247*, 3601−3607.
(12) Wilks, A.; Torpey, J.; Ortiz de Montellano, P. R. *J. Biol. Chem.* **1994**, *269*, 29553−29556.
(13) Davydov, R.; Kofman, V.; Fujii, H.; Yoshida, T.; Ikeda-Saito, M.; Hoffman, B. M. *J. Am. Chem. Soc.* **2002**, *124*, 1798−1808.
(14) Zhu, Y.; Silverman, R. B. *Biochemistry.* **2008**, *47*, 2231−2243.
(15) Mansfield Matera, K.; Takahashi, S.; Fujii, H.; Zhou, H.; Ishikawa, K.; Yoshimura, T.; Rousseau, D. L.; Yoshida, T.; Ikeda-Saito, M. *J. Biol. Chem.* **1996**, *271*, 6618−6624.
(16) Liu, Y.; Moenne-Loccoz, P.; Loehr, T. M.; Ortiz de Montellano, P. R. *J. Biol. Chem.* **1997**, *272*, 6909−6917.
(17) Sakamoto, H.; Omata, Y.; Palmer, G.; Noguchi, M. *J. Biol. Chem.* **1999**, *274*, 18196−18200.
(18) Liu, Y.; Ortiz de Montellano, P. R. *J. Biol. Chem.* **2000**, *275*, 5297−5307.
(19) Balch, A. L.; Latos-Grażyński, L.; Noll, B. C.; Szterenberg, L.; Zovinka, E. P. *J. Am. Chem. Soc.* **1993**, *115*, 11846−11854.
(20) Balch, A. L.; Koerner, R.; Latos-Grażyński, L.; Noll, B. C. *J. Am. Chem. Soc.* **1996**, *118*, 2760−2761.

(21) Kalish, H.; Camp, J. E.; Stępień, M.; Latos-Grażyński, L.; Balch, A. L. *J. Am. Chem. Soc.* **2001**, *123*, 11719−11727.
(22) Rath, S. P.; Olmstead, M. M.; Balch, A. L. *Inorg. Chem.* **2004**, *43*, 7648−7655.
(23) Rath, S. P.; Olmstead, M. M.; Balch, A. L. *J. Am. Chem. Soc.* **2004**, *126*, 6379−6386.
(24) Rath, S. P.; Olmstead, M. M.; Balch, A. L. *Inorg. Chem.* **2006**, *45*, 6083−6093.
(25) Kamachi, T.; Shestakov, A. F.; Yoshizawa, K. *J. Am. Chem. Soc.* **2004**, *16*, 3672−2673.
(26) Gheidi, M.; Safari, N.; Zahedi, M. *Inorg. Chem.* **2012**, *51*, 12857−12866.
(27) Gheidi, M.; Safari, N.; Zahedi, M. *Inorg. Chem.* **2012**, *51*, 7094−7102.
(28) Lad, L.; Schuler, D. J.; Ortiz de Montella, P. R.; Poulos, T. L. *J. Biol. Chem.* **2003**, *278*, 7834−7843.
(29) Lad, L.; Ortiz de Montellano, P. R.; Poulos, T. L. *J. Inorg. Biochem.* **2004**, *98*, 1686−1695.
(30) Gheidi, M.; Safari, N.; Zahedi, M. *J. Mol. Model.* **2010**, *16*, 1401−1413.
(31) Frisch, M. J.; Trucks, G. W.; Schlegel, H. B.; Scuseria, G. E.; Robb, M. A.; Cheeseman, J. R.; Zakrzewski, V. G.; Montgomery, J. A., Jr.; Stratmann, R. E.; Burant, J. C.; Dapprich, S.; Millam, J. M.; Daniels, A. D.; Kudin, K. N.; Strain, M. C.; Farkas, O; Tomasi, J; Barone, V.; Cossi, M.; Cammi, R.; Mennucci, B.; Pomelli, C.; Adamo, C.; Clifford, S.; Ochterski, J.; Petersson, G. A.; Ayala, P. Y.; Cui, Q.; Morokuma, K.; Malick, D. K.; Rabuck, A. D.; Raghavachari, K.; Foresman, J. B.; Cioslowski, J.; Ortiz, J. V.; Stefanov, B. B.; Liu, G.; Liashenko, A.; Piskorz, P.; Komaromi, I.; Gomperts, R.; Martin, R. L.; Fox, D. J.; Keith, T.; Al-Laham, M. A.; Peng, C. Y.; Nanayakkara, A.; Ghonzalez, C. V.; Challacombe, M. W.; Gill, P. M.; Johnson, B. G.; Chen, W.; Wong, M.; Andres, J. L.; Head-Gordon, M.; Replogle, E. S.; Pople, J. A. *Gaussian 03*, revision A.1; Gaussian, Inc.: Pittsburgh, PA, 2003.
(32) Parr, R. G.; Yang, W. *Density Functional theory of atoms and molecules*; Oxford University Press : Oxford, U.K., 1989.
(33) Cramer, C. J. *Essentials of Computational Chemistry: Theories and Models*; Wiley: Chichester, U.K., 2002.
(34) Swart, M. *J. Chem. Theory Comput.* **2008**, *4*, 2057−2066.
(35) Güell, M.; Luis, J. M.; Solà, M.; Swart, M. *J. Phys. Chem. A* **2008**, *112*, 6384−6391.
(36) Roos, B. O.; Taylor, P. R.; Siegbahn, P. E. M. *Chem. Phys.* **1980**, *48*, 15.
(37) Mödl, M.; Dolg, M.; Fulde, P.; Stoll, H. *J. Chem. Phys.* **1997**, *106*, 1836.
(38) Paulsen, H.; Duelund, L.; Winkler, H.; Toflund, H.; Trautwein, A. X. *Inorg. Chem.* **2001**, *40*, 2201−2203.
(39) Reiher, M. *Inorg. Chem.* **2002**, *41*, 6928−6935.
(40) Lee, C.; Yang, W.; Parr, R. G. *Phys. Rev. B* **1988**, *37*, 785−789.
(41) Vosko, S. H.; Wilk, L.; Nusair, M. *Can. J. Phys.* **1980**, *58*, 1200−1211.
(42) Stephens, P. J.; Devlin, F. J.; Chabalowski, C. F.; Frisch, M. J. *J. Phys. Chem.* **1994**, *98*, 11623−11627.
(43) Yoshizawa, K.; Kamachi, T.; Shiota, Y. *J. Am. Chem. Soc.* **2001**, *123*, 9806−9816.
(44) Shiota, Y.; Yoshizawa, K. *J. Am. Chem. Soc.* **2000**, *122*, 12317−12326.
(45) Wittbrodt, J. M.; Schlegel, H. B. *J. Chem. Phys.* **1996**, *105*, 6574−6577.
(46) Groenhof, A. R.; Swart, M.; Ehlers, A. W.; Lammertsma, K. *J. Phys. Chem. A* **2005**, *109*, 3411−3417.
(47) Wong, M. W.; Frisch, M. J.; Wiberg, K. B. *J. Am. Chem. Soc.* **1992**, *114*, 1645−1652.
(48) Sun, J.; Loehr, T. M.; Wilks, A.; Ortiz de Montellano, P. R. *Biochemistry* **1994**, *33*, 13734−13740.
(49) Ito-Maki, M.; Ishikawa, K.; Matera, K. M.; Sato, M.; Ikeda-Saito, M.; Yoshida, T. *Arch. Biochem. Biophys.* **1995**, *317*, 253−258.
(50) Ikeda-Saito, M.; Hori, H.; Andersson, L. A.; Prince, R. C.; Pickering, I. J.; George, G. N.; Sanders, C. R.; Lutz, R. S.; McKelvey, E. J.; Mattera, R. *J. Biol. Chem.* **1992**, *267*, 22843−22852.
(51) Bogumil, R.; Maurus, R.; Hildebrand, D. P.; Brayer, G. D.; Mauk, G. *Biochemistry* **1995**, *34*, 10483−10490.
(52) Ghosh, A. *J. Biol. Inorg. Chem.* **2006**, *11*, 671−673.
(53) Ghosh, A. *J. Biol. Inorg. Chem.* **2006**, *11*, 712−724.
(54) Tangen, E.; Conradie, J.; Ghosh, A. *J. Chem. Theory Comput.* **2007**, *3*, 448−457.
(55) Ktagawa, T. In *Biological applications of Raman spectroscopy*; Spire, T. G., Ed.; Wiley: New York, 1988; Vol. *111*; pp 97−131.
(56) Morishima, I.; Fujii, H.; Shiro, Y.; Sano, S. *Inorg. Chem.* **1995**, *34*, 1528−1535.
(57) Poulos, T. L.; Johnson, E. F. In *Cytochrome P450: Structure, Mechanism, and Biochemistry*; Ortiz de Montellano, P. R., Ed.; Kluwer Elsevier: New York, 2005; pp 87−114.
(58) Shaik, S.; Kumar, D.; de Visser, S. P.; Altun, A.; Thiel, W. *Chem. Rev.* **2005**, *105*, 2279−2328.
(59) Harris, D. L.; Loew, G. H.; Waskell, L. *J. Am. Chem. Soc.* **1998**, *120*, 4308−4318.
(60) Jensen, K. P.; Ryde, U. *J. Biol. Chem.* **2004**, *279*, 14561−14569.
(61) Wasbotten, I.; Ghosh, A. *Inorg. Chem.* **2006**, *45*, 4914−4921.